SOLUTION MINING
RESEARCH INSTITUTE
1745 Chris Court
Deerfield, Illinois 60015-2079
USA
Telephone: 847-374-0490 ◆ Fax: 847-374-0491
E-mail: bdiamond@mcs.com

Meeting Paper

Corrosion Protection of Steel Pipelines in Brine Service by Internal Concrete Liners

by

T. E. Hinkebein
L. P. Montes
L. M. Maestas
Sandia National Laboratories
Albuquerque, New Mexico 87185, USA

R. G. Buchheit
Department of Material Science and Engineering
The Ohio State University
Columbus, Ohio 43210, USA

J. L. Maldonado
Strategic Petroleum Reserve Project Management Office
Department of Energy
New Orleans, Louisiana 70123, USA

Fall 1998 Meeting
Rome, Italy
4-7 October 1998

CORROSION PROTECTION OF STEEL PIPELINES IN BRINE SERVICE BY INTERNAL CONCRETE LINERS

T.E. Hinkebein, L. P. Montes, L. M. Maestas
Sandia National Laboratories
Albuquerque, New Mexico 87185

R. G. Buchheit
Department of Material Science and Engineering
The Ohio State University
Columbus, Ohio 43210

J. L. Maldonado
Strategic Petroleum Reserve Project Management Office
Department of Energy
New Orleans, Louisiana 70123

ABSTRACT

The performance of concrete materials for internal pipeline protection against the erosive and corrosive effects of flowing brine was evaluated for seventeen different liner formulations. Corrosion rates were measured by linear polarization on samples exposed in a test manifold to flowing brine. Samples were also exposed to static site-generated brine as a function of time. These samples were returned to the laboratory for visual analysis of damage, and examination of brine penetration through the concrete by electron probe microchemical analysis. The study focused on the performance of two liners applied by centrifugal casting: an oil-field-standard calcium silicate-based concrete, and a high-sulfate-resistance calcium-aluminate cement. The study also focused on a calcium-aluminate concrete liner applied by hand. Results showed that standard calcium silicate concrete (API RP10E) and a rotary calcium aluminate concrete provided excellent protection. Pipewall corrosion rates were reduced from 10 to 15 mils per year to 1 mil per year or less. The hand-applied liners also reduced the pipewall corrosion rate, but not to the same degree as the cast liners.

---

*This work was performed at Sandia National Laboratories under contract no. DE-AC04-94AL850

INTRODUCTION

Sandia National Laboratories conducted two related experimental studies as part of the Pipeline Corrosion Control Program, which supports operations of the U.S. Strategic Petroleum Reserve (SPR). In both studies, a variety of concrete lining materials and corrosion measurement techniques were evaluated to enhance the lifetime of steel pipelines used for brine service.

The first study was initiated at Big Hill in April 1992 where 17 different materials were evaluated at conditions representative of the working environment. Electrochemical corrosion rates were measured for these materials both in a test manifold, or flow loop, and in a non-flowing environment. Four years of corrosion-rate data were accumulated, permitting the evaluation of the liner formulations, the application methods and the measurement technique. Additionally cumulative immersion testing was used to evaluate the liner performance visually and micro-chemically.

The second study arose from a unique opportunity to conduct electrochemical impedance spectroscopy (EIS) corrosion measurements on a fully operational low-pressure brine header. Special probes were designed and installed along the 2000-foot header at the time of construction of the West Hackberry header in July 1994. Two concrete chemistries were selected based on the results of the Big Hill study. This study provided an opportunity to evaluate the suitability of electrochemical testing for pipeline corrosion monitoring and has provided insights into the strengths and weaknesses associated with internal concrete lining for SPR pipelines.

MATERIALS SELECTION, DESCRIPTION AND PREPARATION FOR BIG HILL CORROSION MONITORING

Internal concrete lining by rotary application. Internal concrete linings were applied to steel pipe sections using commercially available methods and materials. Plain carbon steel pipe sections (Grade 1020) with a 76-mm (3-in) inner diameter were prepared for lining by sandblasting the pipe interior just prior to liner application.

Fabrication was conducted at Permian Enterprises, Odessa, TX using their standard centrifugal casting production methods (Figure 1) [1]. A variety of different concrete compositions were applied, but all were prepared in a similar manner. The ingredients for all concretes were combined in a mixing bin, then pumped through a delivery lance into the pipe section. The pipe section was capped at one end, and the concrete was pumped through the lance as it was withdrawn. The concrete delivery rate and lance removal rate were chosen to deliver enough concrete for a uniform 12.5-mm-thick (0.5-in) liner in each pipe joint. After charging the pipe section with concrete, the remaining end of the pipe was capped, and the section was loaded onto rollers for the spin-casting operation. Pipe sections were spun at greater than 20g for 1.5 to 4 minutes. This generated forces in excess of 20 g. After spinning, individual pipe sections were removed from the rollers, the ends were uncapped, and excess water and fluid additives were drained from the pipes. This results in a very small water-to-cement ratio. Pipe sections were then kiln cured at 150 ^{o}F for approximately 18 hours, except for one calcium aluminate concrete pipe section, which was cured at ambient temperatures 15±5°C (60±10^{o}F).

Figure 1. Centrifugal application of an internal concrete liner at Permian Enterprises, Odessa, TX.

The nominal compositions of the concrete materials used in this study are given in Table 1. Brief descriptions of the materials used, and the rationale for their selection are provided below.

Table 1.
Nominal concrete compositions for the concrete materials used in this study.

ID	Nominal composition
1	[a]API class C high sulfate resistance Portland cement + 40 w/o class F fly ash (Baseline)
2	[b]Baseline + 4.9w/o latex
3	Baseline + 10.5w/o latex
4	Baseline + 15 w/o latex
5	90% class C Portland cement + 10% fly ash
6	75% class C Portland cement + 25% fly ash
7	45% class C Portland cement + 55% fly ash
8	low sulfate resistance Portland cement + 40% fly ash
9	medium sulfate resistance Portland cement + 40% fly ash
10	Baseline, hand-trowel application
11	Baseline + 0.67% sodium nitrite
12	Baseline + 1.33% sodium nitrite
13	Baseline + 2.00% sodium nitrite
14	[c]Aluminate concrete, kiln cured
15	Aluminate concrete, air cured
16	[d]Baseline + 23% epoxy
16A	Baseline + 10% epoxy

[a]all Portland cements are API Class C and all fly ash is silica fume ASTM Class F
[b]latex additions were a styrene-butadiene co-polymer emulsion
[c]aluminate concretes were Ciment Fondu modified with sized graded alumina aggregate
[d]epoxy additions were Rhone- Poulenc two part epoxies curable in the presence of water

API RP10E "baseline" concrete. A concrete material conforming to American Petroleum Institute recommended practice 10E (API RP10E) was designated the baseline concrete in this study. This material is composed of class-C-high-sulfate-resistance Portland cement (0% C_3A)[†], qualified for sulfate-containing brine environments, with 40% by weight American Society for Testing and Materials class-F silica fume fly-ash aggregate. The average fly-ash aggregate particle size was 0.01 mm (0.4 mils). Fly ash has cementitious properties and contributes chemical resistance, strength and reduced permeability to Portland cement. This material has demonstrated excellent performance in oil-field applications and is considered an industry standard material [2].

Hand-trowel application of concrete liners. Spool pieces including tees, elbows, flanged sections, and reducers cannot be lined using rotary methods because of their shapes. These parts must be lined by hand (Figure 2). For hand-trowel application, the as-applied concrete mortar contains more water than is present for rotary-applied mortar. After curing, hand-trowelled liners are less dense than liners applied using rotary methods. As a result, these liners are more permeable and have lower strength than rotary-applied liners.

Figure 2. Hand-trowel application of an internal concrete liner on a spool piece for the 24" brine header at West Hackberry.

Polymer-modified concretes. Epoxy and latex polymer additions to Portland cement concretes are known to improve mechanical properties and retard abrasion and permeation by fluids. For these reasons, polymer-modified concretes were selected for study [3]. A latex emulsion

[†] Cement chemist's notation is used when referring to cement chemistry (see Appendix A). Standard chemist's notation is used otherwise.

specifically manufactured for use in concretes was obtained from Dow Chemical Company. This material was a styrene-butadiene co-polymer emulsion, known as Modifier A. Nominal additions of 5, 10 and 15% were intended. However, the amount of emulsion retained in the concrete layer was reduced by differential segregation that occurred in the centrifugal casting operation. Much of the emulsion was rejected during rotary casting and was eliminated with excess water. As shown in Table 3, the specific gravity of each material measured after curing was nearly identical, but was lower than that for the baseline material. This result shows that the latex emulsion was retained in a rotary-applied liner, but the loading level was determined by the rotation rate during the casting procedure and not by the initial loading level.

Table 3.
Concrete mixes and densities for the latex-modified concretes used in this study.

Material	Cement (kg)	Fly Ash (kg)	Latex Emulsion (kg)	Density (g/cm^3)
Baseline	136	91	0	2.45±0.07
5% Latex	136	91	14	2.22±0.06
10% Latex	136	91	27	2.24±0.02
15% Latex	136	91	41	2.24±0.02

Epoxy additions to the Portland cement were made with a two-part epoxy system capable of curing in the presence of water. The epoxy was obtained from Rhone-Poulenc and consisted of Epi-Cure 872, an amido-amine accelerated curing agent, and Epi-Rez WD-510, a liquid bisphenol epoxy resin. Resin and hardener were mixed per manufacturer's instructions, added to the concrete mixing bin, and then mixed thoroughly before injection into the pipe section. As with the latex additions, the polymer loading level was difficult to control and only some of the epoxy was retained in the liner after centrifugal casting.

Portland cement/fly ash variants. Four concretes were prepared with different cement-to-fly-ash ratios. The ratios selected were: 90:10, 75:25, 60:40, and 45:55 percent by weight. These variations were examined because fly-ash additions affect liner strength and resistance to environmental attack. Positive effects reported for increasing concentrations of fly ash include increased strength, reduction in drying shrinkage, reduction in permeability, and improved resistance to sulfate attack [4]. Negative effects reported for increasing concentrations fly ash include decreased resistance to carbonation and lower concrete pH (lower protective capacity for underlying steel) [5]. This range of compositions was selected to verify that the 60:40 Portland-to-fly-ash mixture was suitable for SPR applications.

Sulfate-resistant Portland cement variants. Low sulfate resistance, moderate-sulfate-resistance, and high-sulfate resistance Portland cements were included in the study to assess their performance during exposure to SPR-generated brine. Brine disposal lines are exposed to solutions whose dissolved sulfate content varies from 0 to 2000 ppm [6]. The susceptibility of a silicate cement, like Portland, to sulfate attack depends on the amount of tricalcium aluminate, C_3A, in the dry cement. Soluble sulfates react with C_3A in hydrated cement leading to reactions whose products form with a volume expansion. This results in softening and spalling of the concrete. The American Concrete Institute recommends the use of high-sulfate-resistance Portland cements (API class C) for service where sulfate concentrations are in excess of 1500 ppm.

Aluminate cements and concretes. Calcium aluminate (CA) concretes were included in this study because they are resistant to chemically aggressive environments [7,8,9]. These materials are especially noted for their resistance to sulfate attack. Aluminate liners can be applied using the same methods and apparatus used for the Portland cement-based liners. Nominal compositions of aluminate cements and the baseline Portland cement are given in Table 4.

Table 4.

Nominal compositions (by weight percent) for Portland cement and calcium aluminate cements.

Cement Type†	S (SiO_2)	C (CaO)	A (Al_2O_3)	F (FeO_x)	S ($CaSO_4$)
Portland	21	63	6	3	3.5
Calcium Aluminate	4	37	40	18	--

Cement chemist's notation on top; corresponding chemical compound in parentheses.

An additional issue relevant to SPR applications is the phenomenon of conversion. At ambient temperatures, the low-density phase CAH_{10} will decompose or "convert" over time to the high-density phase C_3AH_6 with the liberation of water according to the reaction

$$3CAH_{10} \rightarrow C_3AH_6 + 2AH_3 + 18H \ .$$

This process occurs with an increase in porosity and a decrease in strength. The kinetics and mechanisms of hydration and conversion are complicated and depend on a variety of factors. These factors include the water-to-cement ratio (which is extremely low after spinning), concrete porosity (different for rotary versus hand-trowel application), and the effect of the presence and concentration of iron oxides (variable from vendor to vendor).

The calcium aluminate lining material selected for the Big Hill study was obtained from LaFarge Aluminates, Inc., Norfolk, VA. The calcium aluminate cement was mixed with sized graded alumina (Al_2O_3) aggregate prior to injection into the pipe sections. As shown in Figure 3b, the centrifugal casting operation segregated large particles near the steel-concrete interface and fine particles toward the inner liner interface.

Two calcium aluminate liners were prepared. The first was cured at ambient temperatures to promote formation of the high-strength, but unstable-phase CAH_{10}. The second was cured at 66°C (150°F) to promote the formation of the lower strength, but stable C_3AH_6.

Baseline concrete plus corrosion inhibitors. Concrete liners prepared with corrosion inhibitors were tested as a means of slowing corrosion of steel at the steel-concrete interface. A common corrosion inhibitor used to protect steel rebar in concrete is the nitrite anion NO_2^-. Sodium nitrite was added to the baseline concrete in 0.67%, 1.33% and 2.0% levels by weight to determine its ability to slow corrosion of steel at the pipe wall. In the presence of iron, at the conditions of potential and pH existing at the brine-saturated steel-concrete interface, the nitrite anion functions as an oxidizing agent that promotes formation of a protective iron oxide film on iron.

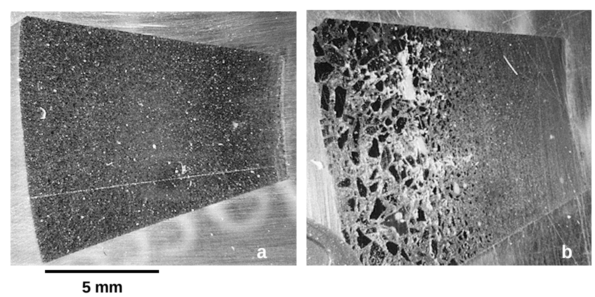

Figure 3. Cross-sectional optical images of the API RP10E liner (a) and the calcium aluminate liner (b). The steel-concrete interface is on the left side of each image; the concrete-brine interface is on the right.

Corrosion-rate measurements at Big Hill. The flow loop was operated from May 1992 to September 1996 to test these concrete liners under simulated service conditions using fluids (brackish water to saturated brine) generated from site operations. Corrosion rates were measured using linear polarization (LP) probes whose sensing surface was situated at the pipe inner diameter (ID). These probes provided a quantitative measure of corrosion rate at a fixed location along a pipe section. Due to space limitations in the flow loop, certain samples fitted with linear polarization probes were immersed in the brine pond under non-flowing (stagnant) conditions.

The flow loop at Big Hill, shown in Figure 4, used a 1900 L/min (500 gpm) pump to withdraw solution from a brine settling pond and pass it through a test manifold containing the pipe test sections. After passing through the manifold and test sections, the solution was deposited back into the settling pond at a point far removed from the manifold intake. The flow rate in the loop was scaled to create the same pipe-wall shear stress that would be experienced by a 0.92 m (36 in) diameter pipe containing solution flowing at 2.4 m/s (7.75 ft/sec).

Figure 4. The flow-loop test manifold at Big Hill.

Corrosion-rate measurements were made using two-element LP probes. Each element was a 1.2 cm^2 (0.186 in^2) plain carbon steel coupon embedded in epoxy and threaded into specially designed fittings welded into the pipe sections. The concrete liner was applied after the probe was inserted into the pipe, ensuring that the element was situated at the steel-concrete interface. The corrosion rate was measured using a commercial meter (Model RCS 9000 Corrater, Rohrback Cosasco Systems, Inc.). Big Hill site personnel made corrosion-rate measurements on a weekly basis.

Big Hill Corrosion-Monitoring Results. Figure 5 is a summary of the corrosion-rate data for the various samples obtained from the LP measurements. The plot shows the mean value, the minimum non-zero value (typically the detection limit of the measurement), and the maximum value for each set of probes. The largest corrosion rates were observed on the bare-steel control samples, which showed nearly identical mean steady-state values for both flowing and stagnant exposure conditions. The average steady-state values ranged from 50 and 60 mpy, which is consistent with the high end of corrosion rate ranges reported in the literature for carbon steel exposed to aerated seawater environments [12,13]. This corrosion rate is significantly greater than the 10 to 15 mpy historical average corrosion rate of bare-steel brine-disposal lines at the SPR. The discrepancy is attributed to the fact that occasionally during the test period, the fluid in the brine pond was diluted with rain water, causing the dissolved salt content to fall and the dissolved O_2 content to increase.

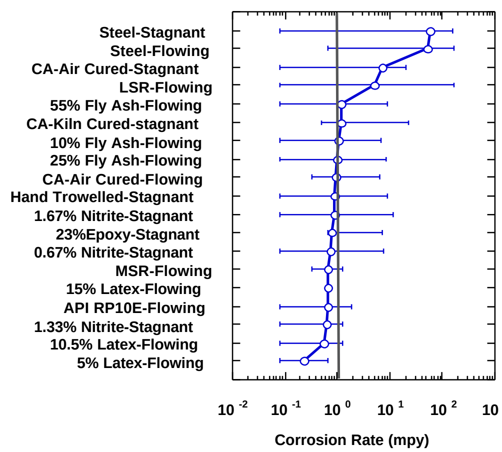

Figure 5. Linear polarization corrosion-rate data summary.

Most of the remaining concrete-lined samples exhibited corrosion rates of about 1 mpy, indicating that the chemistry variations examined did not have a major effect on the corrosion rate of the underlying steel. Post-test examination showed that shrinkage cracks in the concrete were present in the vicinity of LP probes, where higher corrosion rates were measured (e.g. CA-Air Cured-Stagnant and LSR-Flowing). No shrinkage cracks were detected in the vicinity of LP probes where lower corrosion rates were detected (e.g. 5% Latex-Flowing). These results suggest that the degree of shrinkage cracking is significant in determining the degree of liner corrosion protection.

LP probes with small sensing surface areas may give anomalously high corrosion rates if they are located near a shrinkage crack. Conversely, probes located far away from a shrinkage crack may yield anomalously low corrosion rates.

Cumulative immersion testing. Cumulative immersion testing was conducted to track the performance of concrete-lined steel pipe test specimens as a function of exposure time to static SPR-generated effluent. Samples were prepared in the same manner as in the flow-loop experiment. Approximately 650 samples, 75 mm (3 in) in length, representing each of the 17 different materials under test were immersed in the brine pond at Big Hill in April, 1992. Samples were organized into twelve groups. Individual groups were returned to the laboratory for analysis at periodic intervals. Evaluations included visual examination, and microchemical analysis of the concrete liner.

Visual inspection. Visual examination was conducted to check the integrity of both the concrete liner and the underlying steel. The liner was inspected for large-scale changes, such as cracking, softening, spalling or marine growth. The steel-concrete interface was inspected to qualitatively assess the type and degree of corrosion occurring. For examination, a single 75-mm (3 in.) sample was cut in half longitudinally, and the liner was physically removed from one of the halves. Each half was inspected, relevant notes were made, and photographs were taken.

Visual inspection allowed rapid qualitative evaluation of the performance of the concrete liner and the degree of corrosion damage at the steel-concrete interface. Visual inspection showed that over the test period, no spalling or softening (from sulfate attack) had occurred for any of the materials. Cracking was commonly observed due to shrinkage that occurred during curing. Some biofouling of the linings was noted, but bio-deposits were never thicker than 2.0 mm. The fouling was typically uniform across the surface and was black in color. In all samples, except the hand-trowelled baseline material, corrosion at the steel-concrete interface was non-uniform (Figure 6), which is typical for corrosion of plain carbon steel in alkaline-chloride solutions [14]. Overall, the degree of corrosion was slight and pipe wall thinning was negligible, in general agreement with the LP corrosion-rate measurements.

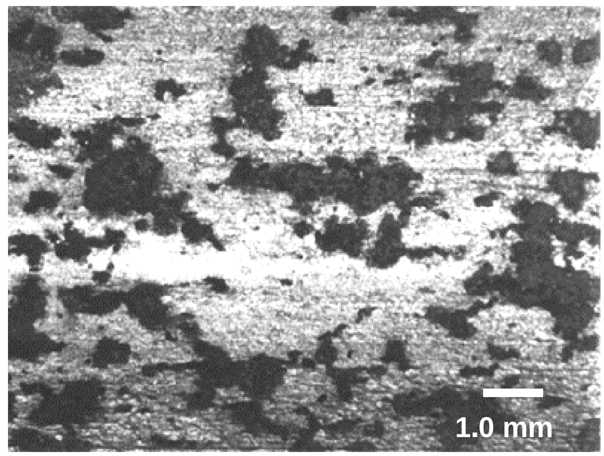

Figure 6. Localized corrosion at the steel-concrete interface.

The performance of hand-trowelled baseline material was detectably inferior to all the other centrifugally-cast liners tested. Corrosion at the steel-concrete interface was uniform but not severe enough to cause loose corrosion product to form. Adhesion of the lining to the steel base was poor. Pipe joint ends finished by hand with mortar also showed severe corrosion damage. It should be expected that in pipelines, damage at the pipe joint end will be compounded by leakage around gaskets at the welded junction.

Electron-probe microchemical analysis (EPMA). EPMA of the concrete liners was used to track permeation of brine and degradation of the cement liners as a function of exposure time in the brine-settling pond. Sections of the internal concrete liner were removed, potted in epoxy and polished for x-ray microanalysis. X-ray linescans were performed using a JEOL 8600 electron microprobe. Analyses were conducted by stepping the beam in 0.05-mm (2-mil) increments from the steel-concrete interface to the concrete-brine interface. Quantitative wavelength-dispersive X-ray data were generated using a 25 nA beam at an accelerating voltage of 15 keV. No changes in concrete constituents were detected. However, chloride from the brine was detected in the concrete materials, and changes in the Cl^- distribution with time were measured.

Figure 7 shows a typical depth profile for chloride from a cross section of a baseline material liner after 4 months' exposure. The trace shows three significant features. The dominant feature was a large concentration of Cl^- detected at the concrete-brine interface, which is due to permeation of brine through the pore space in the cement paste. At positions midway through the liner, small peaks were observed. Microscopic examination of the traced path shows that these occurred at shrinkage cracks in the liner, indicating the brine is preferentially transported along these paths. The third feature was an elevated Cl^- concentration at the steel-concrete interface. This accumulation is due to diffusion of Cl^-, which is facilitated by transport through shrinkage cracks. High concentrations of Cl^- at the interface will cause breakdown of the protective film on the steel, thus promoting corrosion.

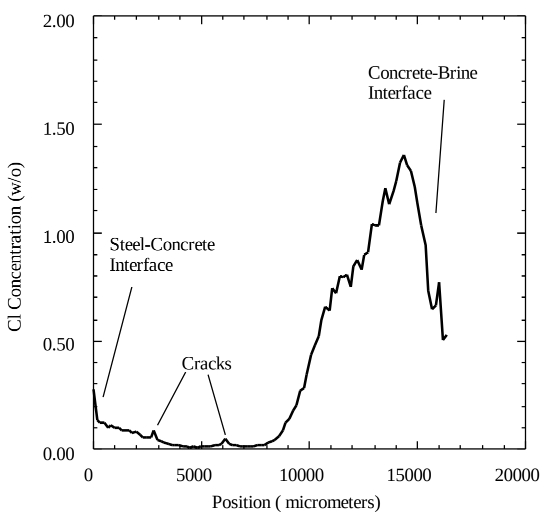

Figure 7. A profile of the chloride ion concentration as a function of position through the baseline material showing typical features observed.

Figure 8 plots the Cl^- concentration in the vicinity of the steel-concrete interface for the baseline and CA concrete liners as a function of exposure time. The data were obtained by integrating the Cl^- concentration over the 2 mm (8 mils) of the liner immediately adjacent to the steel-concrete interface. Units are given in wt%-thickness. The most noteworthy point is the high interfacial chloride concentration for the hand-trowelled concrete compared with the more dense rotary liners. Integrated Cl^- concentrations were slightly lower for the rotary CA liners compared with the rotary baseline material. The jump in signal in all four of the materials after 500 days exposure is due to an increase in the average salinity of the effluent in the brine ponds.

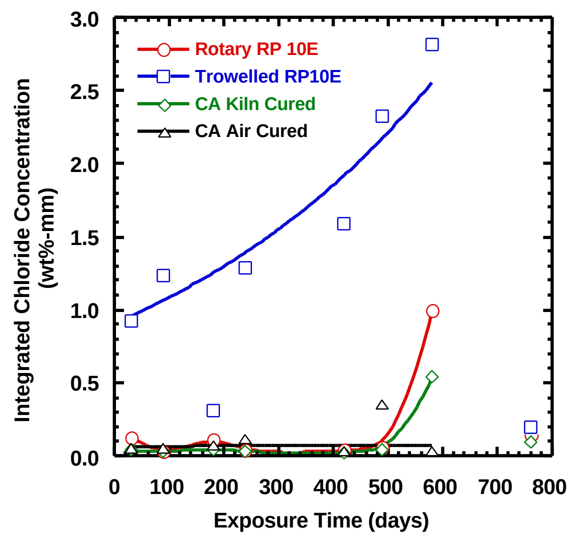

Figure 8. Plot of the interfacial chloride ion concentration as a function of exposure time for the baseline and calcium aluminate materials.

PHASE II CORROSION MONITORING AT THE WEST HACKBERRY SPR SITE

Corrosion monitoring by electrochemical impedance spectroscopy. Electrochemical impedance spectroscopy (EIS) is a powerful tool for making electrochemical measurements. It can provide both kinetic (corrosion rate) and mechanistic information. It is essentially a steady-state measurement, since the applied overvoltages used to make the measurements are never more than a few tens of millivolts away from the steady-state open circuit potential. EIS is well suited for resolving passive corrosion, active corrosion, and diffusion-limited corrosion. The measurement is not invalidated by the large solution resistances that sometimes exist in measurement of steel in concrete. The objective of the monitoring study was to determine:

1) if EIS measurements could be successfully carried out in the field,
2) if EIS was suitable as a long-term corrosion monitoring technique,
3) if EIS yielded corrosion rate data consistent with past and present experience for corrosion of concrete-lined pipelines,
4) if the differences in the corrosion rate and mechanisms of steel pipe with rotary API RP 10E, rotary calcium aluminate, and trowelled calcium aluminate concrete liners.

Probe Configuration and Installation: Specially designed three-electrode probes were built into the pipe sections of the brine header to support EIS measurements. Ten sets of probes were installed on the 0.6-m (24-in) diameter concrete-lined brine header at West Hackberry, which was put into service in July, 1994. The first measurements were performed 3 weeks after the line was put into service.

Probes were installed as diametrically opposed pairs. This was done to ensure that the pipe joint remained balanced during the high-speed centrifugal casting of the liner. A schematic drawing of a probe is shown in Figure 9. Each probe was housed in a 100-mm (4-inch) diameter plain-carbon-steel NPT pipe plug. Three electrodes were circumferentially arranged in each probe. A gold reference electrode was located at the center of the probe, an annular plain carbon steel working electrode (33 cm^2 area (5.1 in^2)) was situated in the middle region of the probe, and a Ni-Cr counter electrode (33cm^2 area) was situated in the outermost position. All three electrodes were potted in an alkaline-resistant epoxy, and electrical connections were run through the probe body to a military connector that was used on the backside for external connections. Threaded weld-o-lets were welded onto the pipe sections and the probes were inserted into these just prior to application of the internal cement lining. Probes were designed so that when fully seated, the sensing surface was flush with the pipe ID (Figure 10).

Materials. Three different liner materials were placed in this brine header for evaluation. They were rotary-applied API RP10E which is an oilfield standard 60%-40% calcium silicate-fly ash aggregate rotary concrete, a rotary calcium aluminate concrete supplied by Lehigh Cement company, and a similar calcium aluminate formulation, applied by hand-trowelling on spool pieces. Three sets of EIS probes were located under each of the rotary liners and 4 sets were located under the hand- trowelled liner.

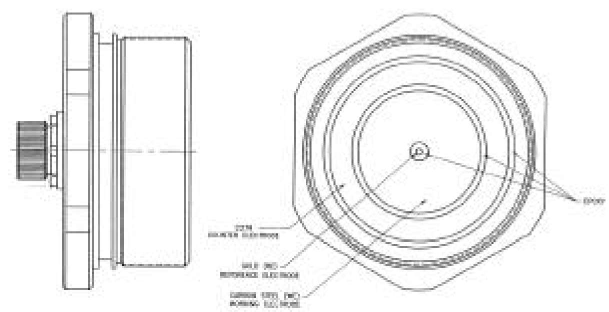

Figure 9. Schematic illustration of the EIS probes for corrosion monitoring at West Hackberry.

Figure 10. An EIS probe installed in a pipe section ready for application of the internal liner.

Corrosion-monitoring methods. EIS measurements were made using standard laboratory equipment set up in minivans for transport along the 2000-foot-long header. Electrical power provided by gas-powered generators was used to run the instrumentation. EIS measurements were typically made using a two-electrode configuration at the open-circuit potential of the working electrode. To combat occasional electrical noise problems, the electrode was potentiostatically polarized to a potential 20 to 30 mV positive of the open-circuit potential during the EIS measurement. A 10- to 20-mV sinusoidal voltage modulation was used, and data were taken at a rate of 4 to 7 points per decade frequency from 10 kHz to 1 mHz. This frequency range was sufficient to capture significant charge transfer and diffusion processes occurring without making the measurements unreasonably long.

Discussion of EIS measurements. EIS data from the probes were of four primary types common for corrosion of steel in concrete [15-18]. Examples are given in complex plane plots of EIS data shown in Figures 11 through 14. Figure 11 shows data obtained from a probe located under a rotary calcium aluminate liner. The data fall along a straight line with a slope of about 2.5. This response is characteristic of passive steel surfaces. Steel is normally passivated by the alkaline conditions created by concrete. Under these conditions, the corrosion rate of the steel is very low (< 0.001 mpy).

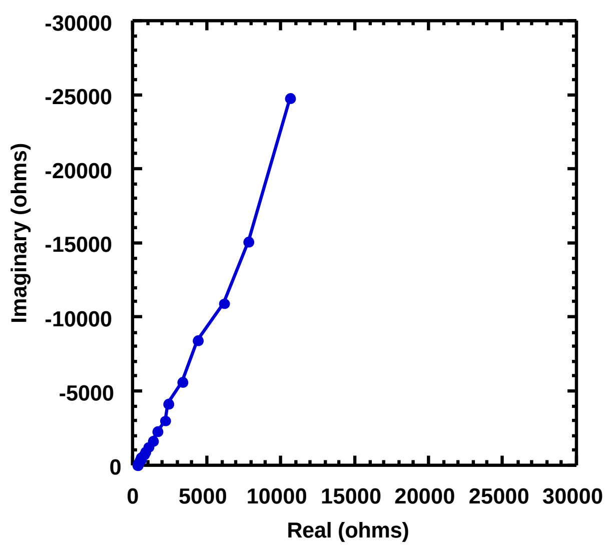

Figure 11. Complex plane plot of EIS data from a probe located under a rotary calcium aluminate concrete liner indicating corrosion through a passivating layer.

When the interfacial chloride concentration becomes sufficiently high, passive film breakdown occurs and active corrosion ensues. Figure 12 shows EIS data obtained from a probe located under rotary API RP10E concrete liner material. The data fall along a depressed semi-circular arc that is characteristic of active corrosion at the steel-concrete interface. Corrosion rates can be directly calculated by extracting a polarization resistance from the data. Corrosion rates have been observed to range from 0.01 to 5 mpy when active corrosion is occurring. The arc is strongly depressed, as the arc center lies well below the real axis. Arc depression is normally attributed to localized corrosion at the steel-concrete interface [19, 20]. Visual inspection of pipeline section samples returned from field exposure show that this is the case here. However, the presence of porous layers at the interface can also produce depression in semi-circular arcs and its influence can not be ruled out in this case [21].

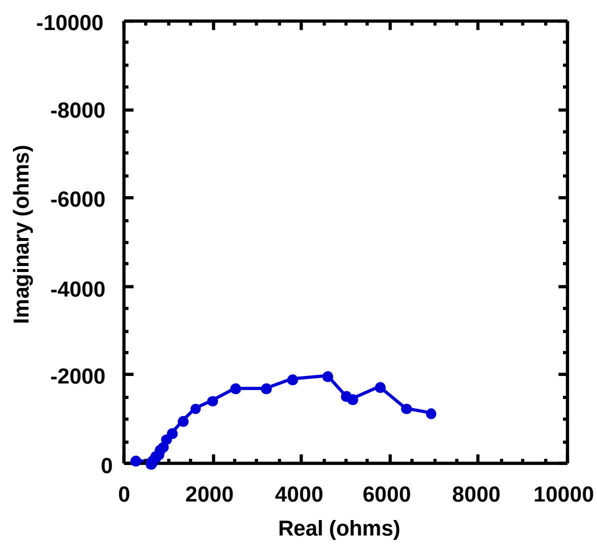

Figure 12. Complex plane plot of EIS data from a probe located under a rotary API RP10E concrete liner indicating that active corrosion is occurring.

Figure 13 shows EIS data obtained from a probe located under a hand-trowelled CA liner. The data fall along a straight line with a slope of one indicating diffusion-controlled corrosion. In this case, the corrosion rate is limited by diffusion of dissolved oxygen to support the corrosion process. In this situation, the impedance curve yields a polarization resistance that is functionally dependent on the effective diffusion coefficient and the diffusion thickness. Corrosion rates are then estimated using the Stern-Geary equation.

In some cases, several different processes were detected in an EIS measurement. Figure 14 shows EIS data obtained from a probe located under a hand-trowelled CA liner. Three processes are evident in this plot. At high frequencies (leftmost data) a small arc is detected. This arc has been attributed to a dielectric response of a non-corrosion product reaction layer that forms at the steel-concrete interface during fabrication [22]. The development of this layer and the degree to which it is detected in EIS measurements depend on the concrete chemistry, the application method and the environment [23]. So far, the presence or absence of this "film effect" has not been correlated with a high or low corrosion rate, or a specific corrosion mechanism. At intermediate frequencies, a larger arc due to active corrosion is observed. At the lowest frequencies, a diffusional response is detected. In this situation, detection of diffusion in the EIS measurement does not necessarily mean that diffusion controls the corrosion rate. The volume of solution trapped at the steel-concrete interface is very small and the chemistry of interfacial region may be perturbed by the measurement. It is therefore possible to locally deplete a reactant during early stages of the measurement, like dissolved oxygen, causing a diffusional limitation to develop in later stages of the measurement. This response is considered to be an artifact of the measurement and not part of the steady-state corrosion process. In these situations, corrosion rates are determined from the arc produced by active corrosion.

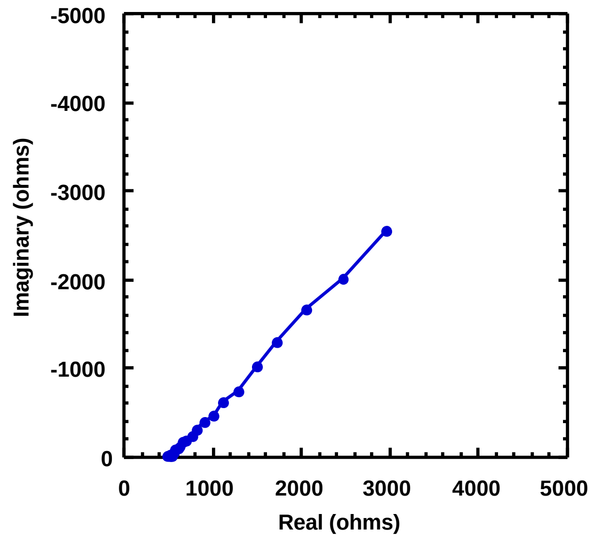

Figure 13. Complex plane plot of EIS data from a probe located under a hand-trowelled calcium aluminate concrete liner indicating that diffusion-control corrosion is occurring.

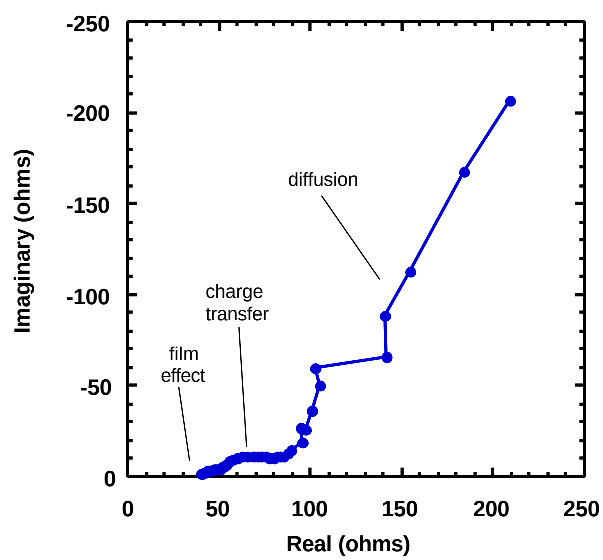

Figure 14. Complex plane plot of EIS data from a probe located under a hand-trowelled calcium aluminate concrete liner showing three different processes.

It is important to distinguish a true diffusional-limitation on the process, like that shown in

Figure 13, from artifact diffusion in Figure 14. In Figure 13, evidence of diffusion is exhibited over the entire frequency range measured (from the beginning to end of the experiment). This suggests that diffusion was operating prior to the beginning of the measurement. This in turn means that a diffusion limitation operated under steady-state conditions and was limiting the rate of the naturally occurring corrosion process.

Corrosion rates were determined by extracting or estimating a polarization-resistance value from the EIS data. Polarization resistance values, R_p, values were determined by fitting the depressed semicircular arc due to the active corrosion process [24]. In cases where a diffusion controls, the impedance curve also yields a polarization resistance. To compute the corrosion rate, R_p was used in the Stern-Geary equation [10]:

$$i = \frac{B}{R_p}$$

where B is a constant equal to 25 mV/decade for corroding steel in concrete [25]. Unit conversion was then used to transform the corrosion rate data to units of mpy.

Figure 15 summarizes the corrosion rate data for hand-trowelled CA, rotary CA, and rotary API RP10E lined pipe obtained in corrosion monitoring at West Hackberry after 1300 days of exposure. Strong time-dependent trends in the data do not appear. Average corrosion rates over this time period have been computed and are shown in Table 1. The performance of the three different liners can be ranked by corrosion performance based on the data in Figure 15 and Table 5. The ranking, in order of decreasing corrosion rate, is

hand-trowelled CA > rotary API RP10E > rotary CA.

Corrosion rates of steel pipe protected by each of these three liners is well below the historical SPR brineline corrosion rates of 10 to 15 mpy.

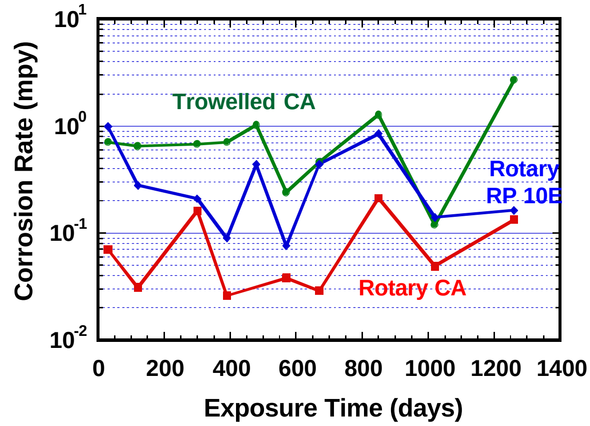

Figure 15. Corrosion-rate data summary from EIS data obtained using the EIS probes at West Hackberry, August 1994 to December 1997.

Table 5. Average corrosion rates for the 0.6 m (24 in) brine header at West Hackberry, August 1994 to April 1997.

Material	Corrosion Rate (mpy) m ± s
Trowelled Calcium Aluminate	0.65±.4
Rotary Baseline	0.39±.3
Rotary Calcium Aluminate	0.08±.1

SUMMARY AND CONCLUSIONS

The studies have been conducted at Big Hill and West Hackberry as part of the Pipeline Corrosion Control Program. These studies have focused on the evaluation of a variety of rotary-applied and hand-applied concrete materials for internal pipeline protection. Additional effort has been dedicated to establishing the viability of electrochemical measurements for monitoring concrete-lined pipe. The primary objective of this program has been to generate a relevant technical information base to support selection of concrete materials for internal protection of SPR pipelines and to provide baseline information for corrosion-monitoring methods. Three main tasks have been accomplished:

1) A corrosion survey of 17 different concrete-liner formulations subjected to simulated service conditions at the Big Hill SPR site has been completed.

2) Cumulative immersion exposure of 17 different concrete-liner formulations has been conducted to examine time-dependent changes in the degree and form of corrosion at the steel-concrete interface, and brine penetration through the concrete liner.

3) Corrosion monitoring by EIS of a low-pressure, concrete-lined brine header at the West Hackberry SPR site has been conducted to demonstrate the suitability of this technique for detecting and measuring corrosion at the steel-concrete interface.

Calcium-aluminate concrete liners applied by hand trowelling appear to be a weak link in the internal lining protection scheme. Higher corrosion rates and greater brine penetration are associated with the use of liners applied in this way. These materials are applied to elbows, tees, flanges and reducers. All of these parts produce changes in flow direction of solution, which can add stress to the liners. As a result, the risk of spalling is likely to be greater for hand-applied liners.

Similarly, risk of spalling is likely to be greater in the vicinity of welded joints; especially where pipe joint ends damaged during handling have been repaired by hand trowelling. The junction of two pipe joints may provide an effective crack that permits brine penetration to the steel-concrete interface, creating the possibility of increased corrosion rates.

During the course of these studies, considerable experience with linear polarization and electrochemical impedance spectroscopy as field corrosion monitoring techniques has been gained. Both techniques appear to provide useful information of corrosion rates and mechanisms. Linear polarization is well suited for monitoring because of the ease in conducting the measurement, the short measurement time, and the ease of data interpretation. EIS provides a more detailed mechanistic picture of the corrosion process, but this information is not necessary in routine monitoring activities. Nevertheless, the EIS technique should still be regarded as a valuable electrochemical monitoring technique suitable for use when more sophisticated corrosion diagnosis is required.

The results of this study show that centrifugally-cast internal concrete liner can significantly reduce the corrosion rate of plain carbon steel pipelines in flowing or stagnant brine solutions. In this study the corrosion rate of lines test sections was reduced from 50 to 60 mpy to about 1 mpy. Among the different concrete formulations studied, there were no significant differences in corrosion resistance that could be equivocally attributed to concrete chemistry. LP corrosion rate measurements did not always agree with visual determination of the degree of corrosion at the steel-concrete interface. Major variations in corrosion rate determined by LP appeared to be due to the relative location of shrinkage cracks that permitted easy access to the steel-concrete interface and the LP probes.

Industry-standard calcium silicate and high sulfate-resistance calcium aluminate concrete liners were studied in some detail. The calcium aluminate liner material may provide some performance advantages over the traditional calcium silicate concrete. However, the slight margin of advantage did not justify their use for spun-application.

REFERENCES

1) B. Jackson, J.F. Armstrong, Mat. Perf., 29 (1990): p. 36.

2) S.H. Kosmatka, W.C. Panarese, Design and Control of Concrete Mixtures, 13th Ed., p. 19, Portland Cement Association, Skokie IL, (1988).

3) S.H. Kosmatka, W.C. Panarese, Design and Control of Concrete Mixtures, 13th Ed., Portland Cement Association, Skokie IL, (1988): p. 193.

4) S.H. Kosmatka, W.C. Panarese, Design and Control of Concrete Mixtures, 13th Ed., Portland Cement Association, Skokie IL, (1988): p. 71.

5) S.H. Kosmatka, W.C. Panarese, Design and Control of Concrete Mixtures, 13th Ed., Portland Cement Association, Skokie IL, (1988): p. 19

6) Daily Meter Reading Data Sheets, Big Hill SPR Site, Winnie, TX, 1990-1991.

7) C.M. George, "Industrial Aluminous Cements," Structure and Performance of Cements, P. Barnes, ed., Applied Science Publishers, New York (1983): p. 415.

8) SewperCoat[††], Product information, LaFarge Calcium Aluminates, Norfolk, VA (1992).

9) Atlas Lumnite & Refcon, Product Information, Bulletin 1-01, Lehigh Cement Company, Allentown, PA, (1994).

10) M. Stern, A.L. Geary, J. Electrochem. Soc., 104 (1957): p. 56.

11) R. Grauer, P.J. Moreland, G. Pini, A Literature Review of Polarisation Resistance Constant (B) Values For the Measurement of Corrosion Rate, NACE, Houston, TX, (1982).

12) Corrosion Data Handbook, B.D. Craig, ed., ASM International, Materials Park, OH (1989): p. 460.

13) Corrosion Data Survey, N.E. Hamner, ed., NACE, Houston, TX (1974): p. 165.

14) J.E. Slater, "Corrosion in Structures", Metals Handbook, Vol. 13, Corrosion, ASM, International, Materials Park, OH (1987): p. 1299.

15) J.A. Gonzales, A. Molina. M.L. Escudero, C. Andrade, Corrosion Sci., 25, 519 (1985).

16) C. Andrade, V. Castelo, C. Alonso, J.A. Gonzales, "The Determination of the Corrosion Rate of Steel Embedded in Concrete by the Polarization Resistance and AC Impedance Methods," p. 43, Corrosion Effect of Stray Currents and the Techniques for Evaluating Corrosion of Rebars in Concrete, ASTM STP 906, V. Chaker, ED., American Society for Testing and Materials, Philadelphia, PA, 1986.

17) K.K. Sagoe-Crentsil, F.P. Glasser, J.T.S. Irvine, Br. Corrosion J., 27, 113 (113).

18) L. Hachani, J. Carpio, C. Fiaud, A. Raharinaivo, E. Triki, Cement and Concrete Research, 22, 56 (1992).

19) K. Hlady, L.M. Callow, J.L. Dawson, Br. Corrosion J., 12, 20 (1980).

20) K.K. Sagoe-Crentsil, V.T. Yilmaz, F.P. Glassner, J. Mater. Sci., 27, 3400 (1992).

21) R deLevie in Advances in Electrochemistry and Electrochemical Engineering, Vol. 6, P. Delahay, Ed., Wiley-Interscience, New York, 1969, p. 329.

22) D.G. John, P.C. Searson, J.L. Dawson, Br. Corrosion J., 16, 103 (1981).

23) J.L. Dawson, "Corrosion Monitoring of Steel in Concrete," Corrosion of Reinforcement in Concrete Construction, A.P. Crane, Ed., Ellis Horwood, Ltd., Chichester, p. 175 (1983).

24) "Basics of Electrochemical Impedance Spectroscopy (EIS)" Application Note AC-1, EG&G Princeton Applied Research.

25) R. Grauer, P.J. Moreland, G. Pini, A Literature Review of Polarisation Resistance Constant (B)

Values For the Measurement of Corrosion Rate, NACE, Houston, TX, (1982).

APPENDIX A: STANDARD CEMENT CHEMIST'S NOTATION

C = CaO	F = Fe_2O_3	N = Na_2O	P = P_2O_5
A = Al_2O_3	M = MgO	K = K_2O	f = FeO
S = SiO_2	H = H_2O	L = Li_2O	T = TiO_2
S' = SO_3	C' = CO_2	C-S-H denotes variable composition	